Cement and Concrete Research 39 (2009) 154–164

Contents lists available at ScienceDirect

Cement and Concrete Research

journal homepage: http://ees.elsevier.com/CEMCON/default.asp

# Simulation of the thermal stress in mass concrete using a thermal stress measuring device

Muhammad Nasir Amin [a], Jeong-Su Kim [a], Yun Lee [b], Jin-Keun Kim [a,*]

[a] Department of Civil and Environmental Engineering, Korea Advanced Institute of Science and Technology (KAIST), 373-1, Guseong-dong, Yuseong-gu, Daejeon, 305-701, South Korea
[b] Department of Architecture, College of Engineering, Ewha Womans University, 11-1, Daehyun-dong, Seodaemun-gu, Seoul, 120-750, South Korea

ARTICLE INFO

*Article history:*
Received 29 August 2007
Accepted 9 December 2008

*Keywords:*
Mass concrete
Thermal stress
Thermal stress device
Degree of restraint
Numerical simulation
Thermal expansion coefficient
Finite element code DIANA

ABSTRACT

An experimental study is conducted to simulate the thermal stresses generated in mass concrete. Accurate prediction of the thermal stresses by analysis is quite difficult particularly at early ages, due to uncertain age-dependent properties of concrete. A series of tests was conducted in which the amount of restraint in a thermal stress device (TSD) was varied. The effect of aging and the amount of restraint on stress development that can occur in realistic structures was evaluated. The influence of the uncertain early-age properties of concrete (i.e., elastic modulus, thermal dilation, autogenous deformation and transitional thermal creep), on the generation of thermal stresses was incorporated using a TSD due to the simultaneous development of temperature and the corresponding stress in a restrained specimen from the very beginning of the process. The effect of various amounts of restraint on the generation of thermal stress was pronounced. Numerical simulations of the thermal stress setup were also performed using the finite element code DIANA to verify and extend the experimental interpretation and to determine the maximum value of restrained stress which would occur under highest level of restraint. Adopting this methodology may simplify the complexity of thermal stress analyses (i.e., more precise 3-D thermal stress analysis can be performed using material properties achieved from 1-D uniaxial tests) due to the difficulty of accurately determining the early-age properties of concrete.

© 2008 Elsevier Ltd. All rights reserved.

## 1. Introduction

The generation of thermal stresses is a well-known and major cause of early-age thermal cracking of massive concrete structures. Thermal stresses are generally caused by the restraining of volumetric deformations shortly after concrete is placed. These types of stresses cause damage to structures or degradation of their structural serviceability. They can also cause a loss of water tightness and durability, especially in marine environments. The complexity of the initial concrete properties is another major problem reported in early-age thermal cracking simulations [1–3]. These include the time of cracking due to the existing inherent variability in both the residual stress and in the development of the tensile strength. Considering the concrete properties that are actually time-dependent along with realistic restraint conditions is important when working to eliminate undesirable cracking in immature concrete and ultimately enhance the service life of concrete facilities. The degree of restraint is considered to be one of the crucial factors involved in the estimation of the early-age cracking of concrete when other parameters are kept constant [4]. Several studies have been performed on common restraint conditions [5–7]. A realistic assessment of the restraint conditions is vital due to the significant effects of these conditions on the generation of cracks.

An experimental approach for reproducing restraint conditions (i.e., the restraint variation that can occur in an actual structure) using TSD in early-age concrete is proposed in this paper [8]. The concept and shape of the TSD are shown in Figs. 1 and 2, respectively. The amount of restraint that may influence the thermal stress and cracking of immature concrete can be changed in the experimental TSD. The concept of higher restrained stresses with a higher amount of restraint [9] is shown in Fig. 3. The problem of very-high-temperature generation, especially in the interior of the structure or at any other location, is achieved more effectively by placing the TSD inside a programmable temperature- and humidity-controlled chamber. The use of a temperature and humidity control chamber in this study is superior to the use of a copper/polyethylene plate in preventing shrinkage in a thermal crack apparatus [10] or to the use of wood/polystyrene for temperature control in a cracking frame [11]. The influence of inherited material variability, such as the evolution of the elastic modulus, the thermal dilation coefficient, transitional thermal creep, or autogenous shrinkage is automatically incorporated in the measurement of thermal stresses.

Numerical simulation of the experimental setup used the finite element code DIANA Ver. 8.1.2. Finite element simulation was used to verify and extend the experimental interpretation for the development

* Corresponding author. Tel.: +82 42 869 3614; fax: +82 42 869 3688.
*E-mail address:* kimjinkeun@kaist.ac.kr (J.-K. Kim).

0008-8846/$ – see front matter © 2008 Elsevier Ltd. All rights reserved.
doi:10.1016/j.cemconres.2008.12.008

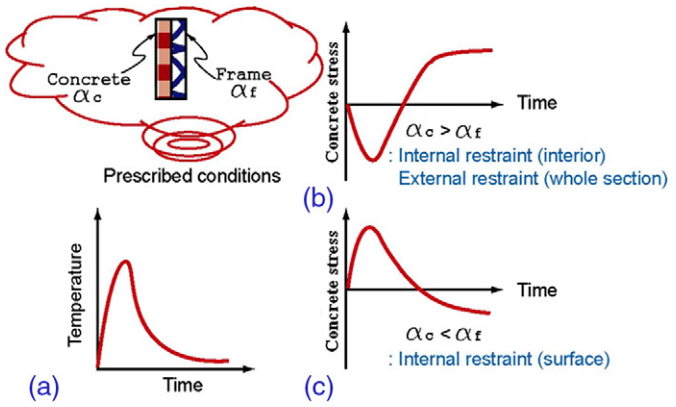


**Fig. 1.** Concept of the thermal stress measuring device: (a) Prescribed temperature history, (b) frame material with a lower thermal expansion coefficient than that of concrete, and (c) frame material with a higher thermal expansion than that of concrete [8].

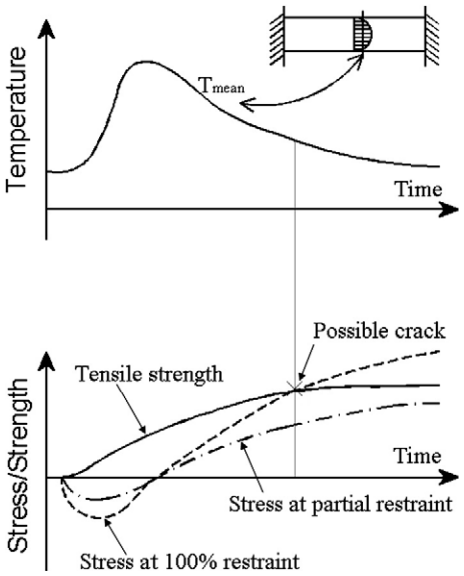


**Fig. 3.** Example of the mean temperature and stress and the strength development in a hardening concrete element restrained both partially and totally (degree of 100%) [9].

of a relationship between the restraint variation and the generation of stress. A parametric study concerning early-age transitional thermal creep behavior and additional experiments using a wider range of various parameters of restraint materials, including the cross-sectional area, stiffness and thermal expansion coefficient, is suggested. Current methodology pertaining to a thermal stress simulation is introduced as more informative and authentic for use in applications.

## 2. Background

### *2.1. Review of laboratory methods used in the measurement of thermal stresses*

Various types of laboratory equipment have been invented in Japan and Europe since the early 1980s to reproduce thermal stress in simulated structures to overcome the shortcomings reported in analytical and experimental techniques. Thermal crack apparatus has been used to investigate hydration heat-induced thermal stresses in concrete, and related mechanisms have been studied [12]. Experimental measurements of the effective modulus of elasticity of mass concrete have been made with a similar apparatus [10]. The cracking frame developed in Germany at the Technical University of Munich (TUM) estimates thermal stresses and cracking patterns in early-age concrete [11,13]. A temperature stress testing machine (TSTM), a modified version of the cracking frame [14,15], was invented based on a cracking frame that can measure restraint forces directly with the help of a built-in load cell and step motors that control the deformation of concrete specimens to a minimum value of 0.001 mm. Variable restraint conditions of 0–100% in accordance with an experimental objective can be achieved using TSTM. Another variable restraint testing machine (VRTM) was built by modifying the TSTM for use under specific conditions [16].

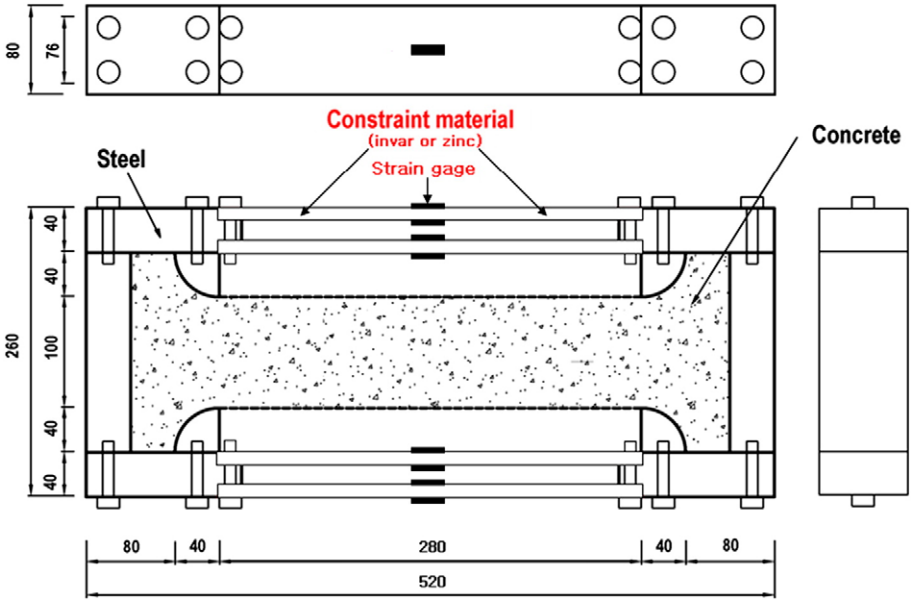


**Fig. 2.** Shape and dimensions of the thermal stress device.

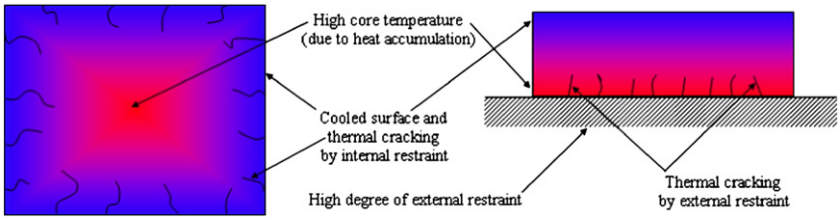


**Fig. 4.** Geometrical representation of the effect of a restraint on stress development and crack occurrence.

The TSD was developed specifically for laboratory uses [8] in view of the drawbacks of other laboratory equipments [10,11]. The coefficient of the thermal expansion of concrete and other cement-based materials is easily controlled using the TSD. Quantitative measurement of the changes in the thermal stresses using the TSD in various environmental and restraint conditions can be done even when the properties of the concrete are uncertain.

### 2.2. General concept of the restraint and generation of thermal stress

A concrete element, if free to move, will have no stress. However, movements of concrete masses are almost always restrained, inducing thermal stresses normally due to temperature variations. When concrete is placed against rigid material, such as a rock foundation, adjoining structures or adjacent older concrete elements, the structure is constrained from moving and strains associated with temperature changes cannot take place. The resulting stress subjected to variation with time is solely due to the adjacent constraint effects or to what is known as an "external restraint". On the other hand, when the temperature field within the section is nonlinear, deformations cannot suit the temperature field and the mechanism is termed an internal restraint. Both internal and external restraints always coexist unless the condition is totally unrestrained. A geometrical representation of combined restraining actions leading to cracking is shown in Fig. 4. Differential thermal gradients in young concrete between the core and the surfaces of the concrete volume and a high degree of base restraint can cause the stress value to cross the tensile strength of concrete.

Cracking mainly depends on the amount or the extent of the degree of restraint (i.e., how much hindrance is offered), as shown in Fig. 3 [9]. This degree of restraint varies between 0 and 100% depending on the physical boundary conditions and on the geometry of the structure. For instance, a full restraint at a concrete rock interface (Kr = 1.0) exists, which gradually decreases as the distance from the interface increases [17].

The widespread use of possibly inaccurate general purely temperature-based criteria has been largely implemented for the purpose of assessing cracking risks [4,18]. The degree of restraint-dependent criteria, however important it may be, has been mostly overlooked or otherwise disregarded in current concrete engineering axioms. It is crucial to realize that the complexity of thermal stress analyses in early-age concrete is of such importance that the monitoring of temperatures as such may never constitute anything but a crude means of controlling cracking in concrete structures [19]. However, 100% restraint has most often been presumed. Little work has been dedicated to the study of the true degree of restraint. The degree of restraint, temperature conditions, thermal dilation, autogenous deformation, and the time-dependent creep/relaxation properties are among important parameters that complicate the determination of early-age thermal stresses and the risk of cracking. Stress is estimated by the constraint factor, which is a function of the geometry and material properties of the concrete and the restraining rock foundation or adjoining structures. A general relationship for the calculation of the tensile stress is

$$\sigma_t = K_r \frac{E}{(1+\phi)} \alpha \Delta T \tag{1}$$

where $\sigma_t$ is the tensile stress, $K_r$ is the degree of restraint, $E$ is the elastic modulus, $\alpha$ is the thermal dilation coefficient, $\Delta T$ is the temperature change and $\phi$ is the creep coefficient.

$K_r$ is determined by comparing the actual strain measured in the field to the strain at the total fixation or by finite element methods [20–22]. The shape and cross-section area of the structure, the geometric properties, the slip occurrences between young and old placings, and their respective elastic modulus values are important parameters that significantly affect restraint variation [17,23].

## 3. Research significance

This research introduces a new methodology of simulation of thermal stress at any location of a concrete structure under well defined temperature and variable restraint conditions using TSD. The temperature conditions of the critical locations can be reproduced by using a programmable temperature- and humidity-controlled chamber. The effects of the varying restraint on the generation of thermal stress were investigated incorporating the uncertain early-age material properties of concrete. The use of the TSD, considering the influence of uncertain material properties under realistic temperature development and an actual time-varying restraint, would provide a superior design of a massive structure free of immature concrete cracking as well as improved data for 3-D thermal stress analyses. A reasonably accurate prediction of the stress development would help in effective control of cracking and reduce cracking risk. Ultimately, this can lead to the design of more durable and safer structures.

## 4. Experimental

### 4.1. Test variables and mix proportions

The composition of concrete ($w/c$ ratio = 0.40, with the average concrete compressive strength at 28 days equal to 40 MPa) and test

**Table 1**
Mix proportion of concrete

| W/C (%) | S/A (%) | Unit content (kgf/m$^3$) | | | | | |
|---|---|---|---|---|---|---|---|
| | | W | C | S | G | Admixture | |
| | | | | | | AE | WR |
| 40 | 39 | 160 | 400 | 726 | 989 | 0.020 | 0.20 |

**Table 2**
Test variables and their mechanical properties

| Type of frame material | Thickness of restraint plate (mm) | Thermal expansion coefficient (×10$^{-6}$/°C) | Elastic modulus (MPa×10$^3$) | Type of restraint condition |
|---|---|---|---|---|
| Invar | 10 | 1.5 | 28.3 | Variable external restraint |
| | 20 | | | |
| | 40 | | | |
| Zinc | 10 | 25 | 108 | Variable internal restraint |
| | 20 | | | |
| | 40 | | | |

variables are listed in Tables 1 and 2, respectively. The values of the mechanical properties are listed in Table 2 regarding the restraining materials of invar and zinc. Concrete cylinders were cast in a $\phi$100 mm×200 mm paper mold and were cured in a chamber under temperature and humidity conditions that were identical to those adopted in the actual thermal stress experiments of this study. Experimental results for three identical specimens were averaged to obtain the standard 28-day compressive strength according to ASTM C 39 and the elastic modulus according to ASTM C 469.

Experiments were conducted for two representative cases: (1) interior of a structure subjected to an external restraint, and (2) surface of a structure subjected to an internal restraint. Invar and zinc were used as restraining materials in TSD to reproduce the state of external and internal restraint, respectively. The tests were repeated for each case after changing the amount of restraint by increasing the thickness of the restraint plate to 10, 20 and 40 mm.

### 4.2. Test equipment

The TSD, originally developed to measure the generation of thermal stress under a prescribed temperature history [8], was used in this study. The shape and dimensions of the device are shown in Fig. 2. The types (external and internal) as well as the varying degrees of restraint in the TSD were achieved by changing the frame material (invar or zinc) and their cross-sectional areas. A commercialized temperature and humidity control chamber was used along with the TSD to reproduce the temperature development of a specific location in structure. The corresponding change of thermal stresses at the specified location was measured quantitatively subjected to various restraint conditions off-setting the uncertain properties of concrete. The variation of the resultant stress was dependent on the thermal expansion coefficient (TEC), the stiffness, and the cross-sectional areas of the frame material when the concrete and the frame material were applied with the same strains under the prescribed temperature history. The following expression was obtained under the same axial displacement condition ($\delta_m=\delta_c$):

$$l_m\left(\alpha_m\Delta T+\frac{F_s}{E_mA_m}\right)=l_c\left(\alpha_c\Delta T+\frac{F_s}{E_cA_c}\right). \tag{2}$$

Here, $l$, $\alpha$ and $E$, denote the length, coefficient of thermal expansion, and elastic modulus, respectively. The subscripts m and c represent the constraint material and the concrete, respectively.

From Eq. (2), the constraint force $F_s$ is expressed as

$$F_s=\frac{l_c\alpha_c-l_m\alpha_m}{(l_m/E_mA_m+l_c/E_cA_c)}\Delta T. \tag{3}$$

As $l_c=l_m$, Eq. (3) can be written as:

$$F_s=\frac{\alpha_c-\alpha_m}{(1/E_mA_m+1/E_cA_c)}\Delta T. \tag{4}$$

In the above equation, the cross-sectional area of concrete $A_c$ remains constant. The constraint force depends only on the difference in the coefficient of the thermal expansions of the concrete and the constraint frame ($\alpha_c-\alpha_m$) and on the axial stiffness of the constraint frame ($E_mA_m/l_m$) if the elastic modulus of concrete remains constant with time.

### 4.3. Experimental procedure

Thermal stresses within concrete specimens varying over time were measured. External and internal restraints were simulated using the restraint materials of invar and zinc, which has thermal expansion coefficients less than and greater than that of concrete ($1.5\times10^{-6}$/°C and $26\times10^{-6}$/°C), respectively. The average strain values in the constraint frame were measured using electric resistance strain gages mounted in the middle of each constraint plate and oriented along the longitudinal axis of the specimen. Three thermocouples were used to ascertain the pre-programmed temperature history in the chamber; one was embedded inside the concrete specimen to measure internal temperature changes while the other two were mounted on the surface of the chamber and on that of the restraint plate, respectively. The programmed temperature history in the chamber was obtained from a prior temperature distribution analysis. The humidity was maintained in excess of 85% inside the chamber throughout the experiment, and all exposed surfaces of the specimen were wrapped with heat-resistant Whatman laboratory sealing film to prevent the evaporation of moisture from escaping the specimen so as to minimize the occurrence of plastic and drying shrinkage. Measurements were determined using a NEC data acquisition system and a personal computer. Restrained stresses were computed after the implementation of temperature compensation measures with a correction of the strain gage values [8].

Mix components, in this case sand, cement, aggregate, and water, were placed inside the chamber at an initially fixed temperature of 20 °C at least one day before mixing to minimize the effect of external factors. The temperature of the mixing room and that of the chamber was maintained at 20 °C during the mixing and placement of the concrete. The left and right surfaces of the specimen (Fig. 2) were covered with thin acrylic plates before the placing of the concrete. These plates were removed 6 h after the placement. The reference points for these values (i.e., the measurement of data started 6 h after the placing of the concrete) were fixed due to the unstable stress and strain conditions that normally occur immediately after the placing of concrete. Friction between the specimen and thin steel bottom plate supporting the frame was minimized by the placement of grease and oil on the bottom plate. The application of lubrication during the test was controlled based on preliminary examinations [8]. A schematic of the setup is shown in Fig. 5.

### 4.4. Experimental results and discussion

#### 4.4.1. Constraint plate (invar) with a thermal expansion coefficient lower than that of concrete

The temperature history measured in the interior of the concrete specimen, on the surface of the constraint plate, and in the chamber showed nearly identical values (Fig. 6(a)). The decision to disregard the hydration heat of cement due to the very thin thickness of the specimen was validated and the pre-programmed temperature history was verified. The TSD, filled with concrete, was placed in the chamber so that a pre-programmed temperature in the chamber could be ensured in the concrete specimen. It was necessary to ensure that


**Fig. 5.** Schematic of the experimental setup.

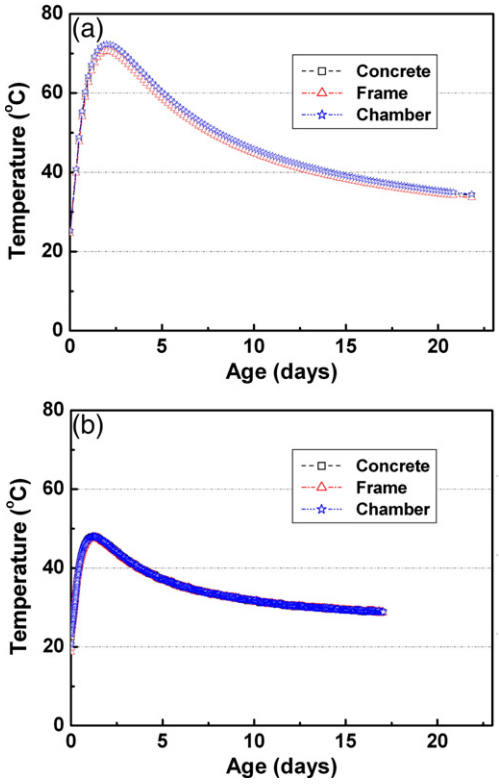


**Fig. 6.** Comparison of the measured temperature histories in the interior and at the surface of the concrete using (a) the invar and (b) the zinc frame.

the temperature of the specimen in the laboratory was equal to when it was a part of the structure, as the concrete specimen acted as a simulated point on the structure. The final stress measured under these conditions corresponded to the thermal stress generated at that location under the simulated restraint condition. The temperature of the specimen increased from its initial temperature to a temperature that exceeded 71 °C at a rapid rate during the first two days. Subsequently, the temperature in the chamber decreased and the specimen began to cool down gradually. Even after 30 days, the temperature in the interior of the concrete specimen was higher than the boundary environmental temperature obtained earlier from a temperature distribution analysis.

The development of stress in the interior of the structure according to different restraint degrees provided by the invar frame is shown in Fig. 7(a). Compression stress developed in the beginning because the concrete tended to expand due to the increase in temperature, while the boundary conditions restrict its expansion. Maximum compression stress occurred at 1.6 days and then decreased as the specimen began to cool down after reaching its maximum temperature. Compression stress continued decreasing from the time it reached its maximum temperature and finally converted to tensile stress after reaching a zero stress condition. During the contraction phase (the decrease in the temperature of the specimen), concrete tends to contract while the boundary conditions restrict its contraction. Generated tensile stress increases continuously as long as the temperature continues to decline. A high level of tensile stress was observed due to the continuous development of elastic properties. The thermal stress generation trend is shown in Fig. 7(a). This trend was similar to the reported variation in the thermal stresses appearing in the interior of mass concrete structures [24].

The degree of restraint had a significant effect on the development of stress (Fig. 7(a)). A thicker constraint plate exhibits a higher level of restraint than a thinner plate. The specimen was likely tested under a higher level of force (i.e., a higher stress-to-strength ratio), which caused the stress level to increase remarkably both in compression and tension. The difference in the measured restrained stress was considerable for constraint plates with thicknesses of 10 and 20 mm and was less pronounced for a thickness between 20 and 40 mm. Earlier cracking of specimens under a higher restraint may explain the smaller difference between plates of 20 and 40 mm despite the similar average stress. The development of micro-cracking in young concrete due to higher restraining tensile stress may also explain these results.

In general, the degree of restraint is always less than 100% and changes with time in realistic structural members due to the variation in the elastic modulus of concrete with time and due to stress relaxation. Restraint provided by a constraint plate with a thickness of 40 mm was assumed to be 100% (i.e., total restraint). Restraints produced by plates 10 and 20 mm in thickness are considered as partial restraints. The ratio of stress (i.e., the stress developed under a partial restraint condition to a total restraint condition) was determined to be 86% and 38% for thicknesses of 20 and 10 mm, respectively (Fig. 8(a)). The stress value decreased markedly as the degree of restraint decreased (i.e., decreasing the restraining amount meant reducing the thickness of the restraint plate). The stress ratio is not equal to the degree of restraint in terms of its value (i.e., for a plate with a thickness of 40 mm, the restraint value was artificially assumed to be equal to 100%, which is correspondingly 50% and 25% for thicknesses of 20 and 10 mm, respectively). Different stress relaxation properties induced by creep under a different degree of restraint may be responsible for this.

It was noted in this case that the restraint on the specimen was relatively weak, as the maximum value of stress under the highest amount of restraint is only 2.18 MPa, which is too small for mass concrete. High early-age creep of concrete, which becomes higher at higher stress levels, may also be a factor that restricted the stress to such a small value. More experimental study is needed using a wider range of restraint material parameters (e.g. the cross-sectional area,

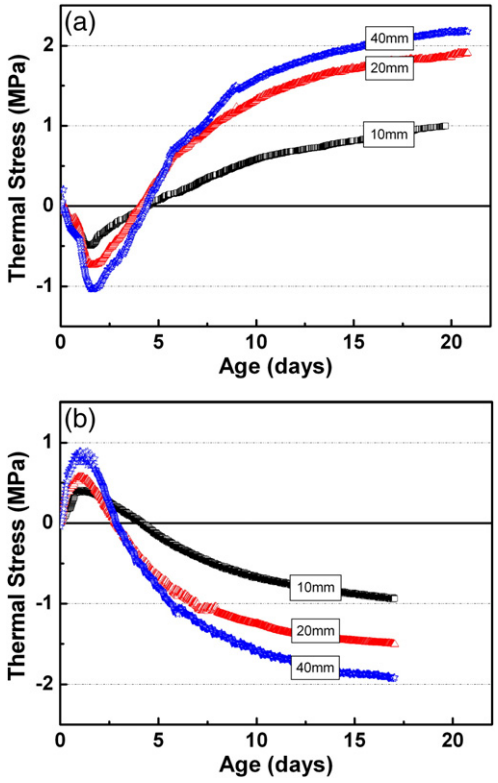


**Fig. 7.** Thermal stress measured over time according to varying thicknesses of the restraint materials (a) invar and (b) zinc.

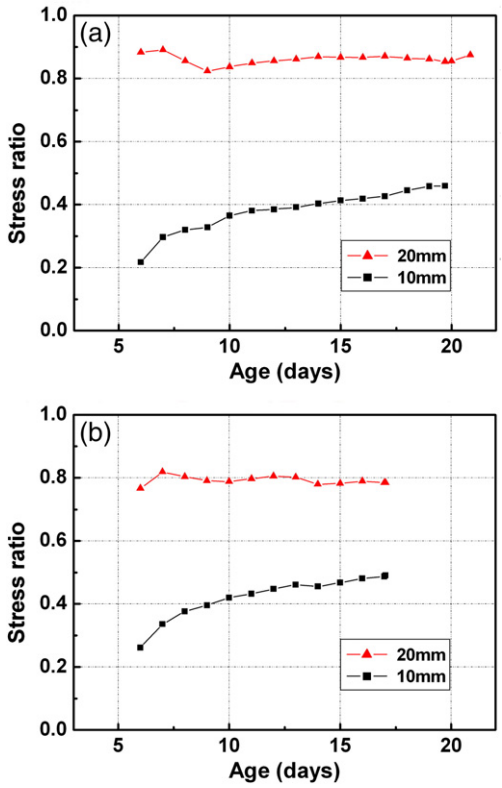


**Fig. 8.** Ratio of stress measured at partial degree of restraint to a presumed total restraint condition (i.e., with the thickness of the frame material equal to 40 mm) according to the restraint materials (a) invar (b) zinc.

stiffness and thermal expansion coefficient). Super-invar 32-5 is expensive but has a very high stiffness value and a lower thermal expansion coefficient ($0.63\times10^{-6}$/°C) than carpenter invar "36" Alloy. Carpenter invar "36" Alloy was used in this study and has a TEC equal to $1.5\times10^{-6}$/°C. A comparison of the thermal expansion curves of both materials at different temperatures is shown in Fig. 9.

*4.4.2. Constraint plate (zinc) with a higher thermal expansion coefficient than concrete*

Test results for the constraint material of zinc are shown in Figs. 6(b) and 7(b). The measurement temperature history at the surface of the concrete specimen, at the constraint plate, and in the chamber showed a considerable amount of similarity, which also validates the decision to disregard the hydration heat of concrete and the pre-programmed temperature history of the chamber (Fig. 6(b)). Test results of the stress measurement using the constraint material zinc are shown in Fig. 7(b). The results exhibit a tendency that is similar to that of the test results of the constraint material invar. However, the thermal stress produced in the beginning is tensile in this case. On contrast, in case of the restraint bar consisting of invar, the thermal stress produced in the beginning was initially compressive due to the restraint of the initial expansion. The differential volume change based on the temperature distribution is restrained by the continuity of the cross-section in a process known as "internal restraint". The test results shown in Fig. 7(b) are similar to the variation of the thermal stresses appearing at the surface of mass concrete structures [25]. The residual compressive stress of concrete (i.e., the part of the curve near the end) shown in Fig. 7(b) can be used to determine residual properties of concrete that are more accurate, which is of great importance as these properties define the best rehabilitation strategy.

Test results of the measured stress ratio for the constraint material zinc are shown in Fig. 8(b). The average residual stress for thicknesses of 20 and 10 mm are 79 and 42%, respectively, of that produced under the falsely assumed totally restraint condition (i.e., 40 mm). The average residual stress was calculated by adding the stress values at each point presented in the graph (Fig. 8(a) and (b)) divided by the total number of points. The values of the average residual stress showed that the stress ratio was not always equal to the degree of restraint in value; however, this may be due to the different stress relaxations induced by creep under different degrees of restraint.

A numerical simulation was carried out using zinc as a restraining material. This was also done for invar. The results of the experiments were reproduced for a restraint bar with a thickness of 40 mm using numerical simulation, and the results were verified later for restraint bars with different thicknesses (10 and 20 mm). Finally, the results of

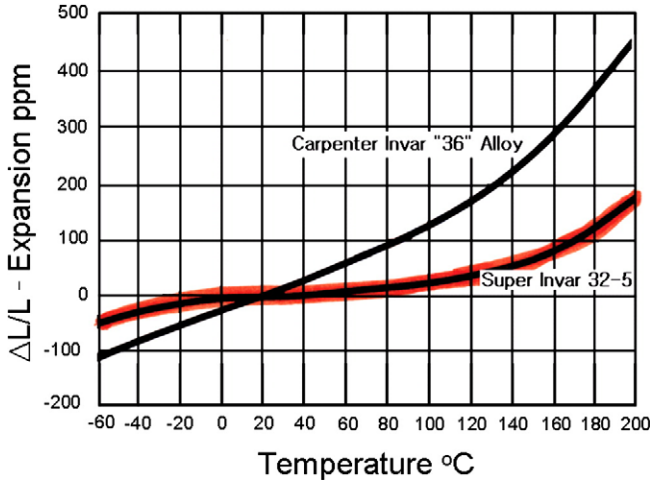


**Fig. 9.** Comparison of thermal expansion curves — Super Invar 32-5 vs. Invar "36" Alloy.

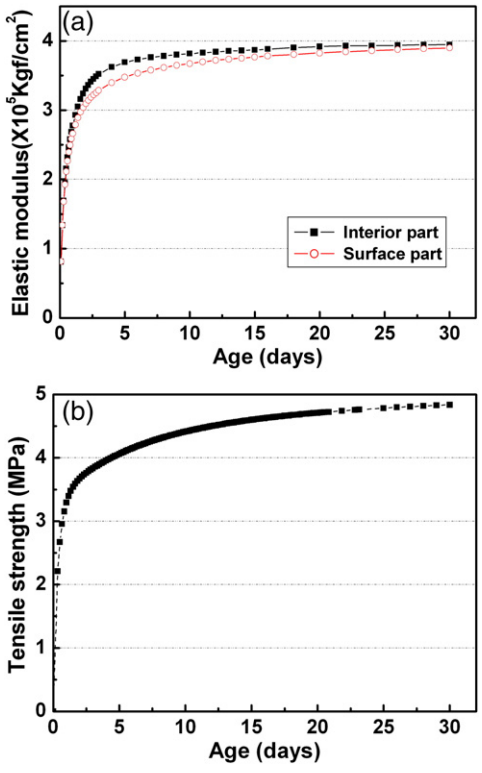


**Fig. 10.** Development of concrete properties over time: (a) elastic modulus in the interior and at the surface of concrete using a different temperature history and (b) tensile strength.

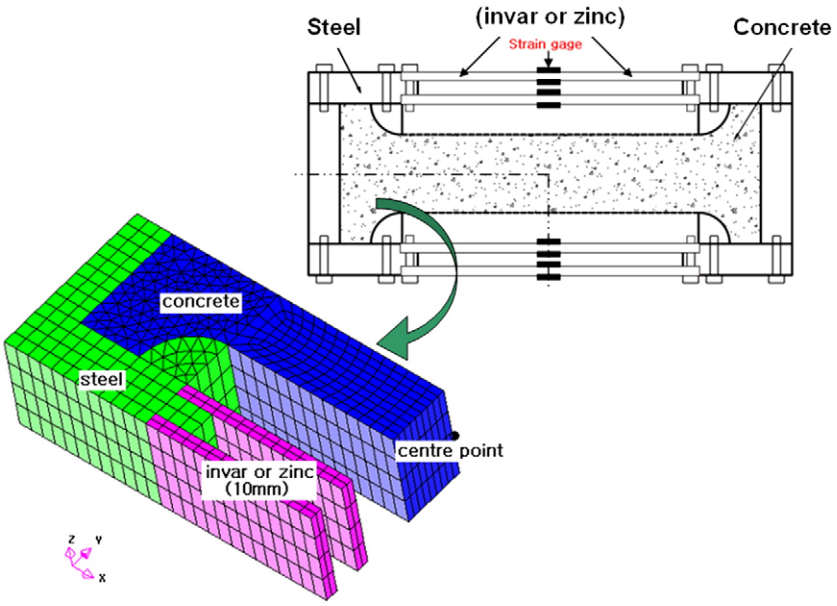


**Fig. 11.** Configuration of the finite element mesh.

the numerical simulation were extended to predict the limiting values of the restraint and the corresponding restrained stresses.

## 5. Numerical simulation of the experimental setup

The maximum value of the measured restrained stress under the highest restraint was 2.18 MPa (for the restraint material invar) which is too small for a typical massive concrete structure. The possibility of an insufficient restraint on concrete and a high degree of early-age creep of concrete, which becomes higher at higher stress levels, were reported as the major factors restricting the stress to such a small value. Numerical simulation of the experimental setup was used to reproduce and extend the interpretation of the test results. The primary objective of the numerical simulation was to evaluate the limiting (or ultimate) values of the restraint and the corresponding restrained stresses. The influences of the restraint amount and a high degree of early-age creep of concrete on the restrained stress were studied.

The experimental setup of the TSD was simulated using the computer code DIANA ver. 8.1.2. A 3-D non-linear thermal stress analysis was carried out. A user-supplied sub-routine was added for the time-dependent elastic modulus (Fig. 10(a)) along with a power-type law [26] to consider the creep effect. The power-type law was chosen due to the ease of performing the analyses with static as well as transient elastic moduli with and without creep. The significance of varying the early-age elastic modulus and creep behavior of young concrete was investigated.

**Table 3**
Thermal and mechanical properties of materials used in the numerical simulation

| Type of properties | Parameters | Concrete | Steel | Invar | Zinc |
|---|---|---|---|---|---|
| Thermal properties | Thermal conductivity (J/day mm$^3$ °C) | 198 | 6932 | 864 | 10368 |
| | Heat capacity (J/mm$^3$ °C × 10$^{-3}$) | 0.00065 | 3.55 | 0.23 | 2.43 |
| | Unit density (kgf/mm$^3$ × 10$^{-9}$) | 2400 | 7850 | 8174 | 6812 |
| | Thermal expansion coefficient (× 10$^{-6}$/°C) | 10 | 10 | 1.5 | 25 |
| Mechanical properties | Compressive strength (MPa) | 40 | – | – | – |
| | Elastic modulus (MPa × 10$^3$) | Transient | 206 | 28.3 | 108 |
| | Poisson's ratio | 0.18 | 0.30 | 0.15 | 0.25 |
| Ambient conditions | Temperature (°C) | Transient | – | – | – |
| | Humidity (%) | 85 | – | – | – |

### 5.1. Methodology

Decoupling of the thermo-mechanical problem is in initial general approach of a thermal analysis. This step is followed by a stress calculation. A coupled flow-stress analysis, considering one-directional interaction, was adopted. The interaction is one-directional for flow and only affects the deformation. Structural analysis with a thermal load is an example of a one-directional interaction of the type that best fits this study. A staggered flow analysis was adopted in which the flow field whose results act as an external load for the subsequent stress analysis was calculated first (i.e., the temperature fields calculated during the first stage acts as an external load for the subsequent stress analysis). The modules LINSTA and NONLIN of DIANA automatically converted the model from a flow to a structural analysis [27].

### 5.2. Modeling and input numerical data

For the sake of simplification, only a quarter of the device was modeled due to the symmetry of the geometry of the TSD (Fig. 11). 20-node brick and 15-node wedge elements were used for the structural analysis, and 4-node BQ4HT and 3-node BT3HT elements were used for the flow analysis as boundary elements. Special interface elements were also used at the boundaries to model the convection. An initial temperature of 25 °C was used at all nodes in the interior geometry, and no heat flow was permitted along the planes of symmetry.

Input data for prior flow analysis (i.e., thermal conductivity, heat capacity, thermal dilation coefficient) along with the environmental conditions are given in Table 3. The temperature fields calculated in the first step of the flow analysis were used as the thermal load for the subsequent transient stress analysis through the built-in function of coupled analysis provided by DIANA. Structural material properties (Table 3) were used in combination with the results of the prior flow analysis as structural material models are applicable in combination

**Table 4**
Parameter values of the power law used in the numerical simulation

| Parameter | Values |
|---|---|
| $P$, power of the creep function | 0.3 |
| $t_d$, is the development point | 15 |
| $\varphi$, creep coefficient | 3.0 |
| $d$, power of the part of the creep function | 0.35 |

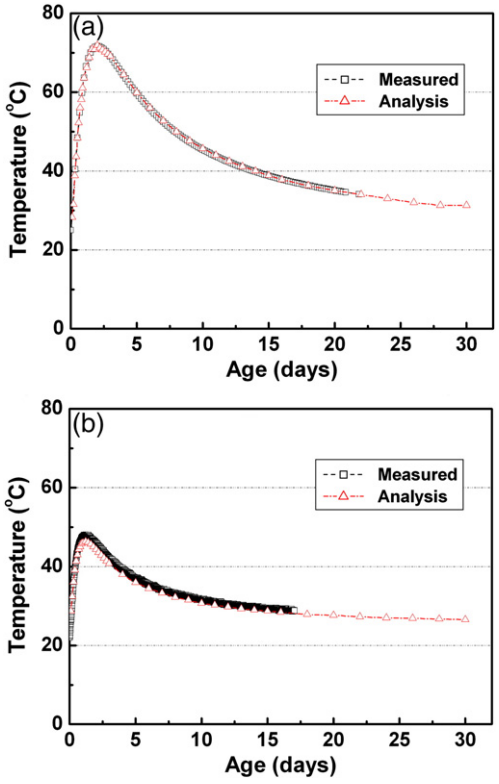


**Fig. 12.** Comparison of the temperature history between the experimental measurement and the numerical simulation for the constraint materials (a) invar and (b) zinc.

with models of the temperature load [27]. The input parameters of the power law used in the analysis are tabulated in Table 4. Finite element calculations were carried out in 40 time steps, starting with increments of 0. 1 day up to increments of 2 day, as the elastic modulus of concrete becomes stable at a later age. The time step was kept small during the hot phase of heat production to model the high gradient heat production during the first 48 h.

### 5.3. Outline of the analysis

Various finite element meshes were generated for each restraint material (invar and zinc) by increasing the transverse thickness from 10 to 200 mm. The thicknesses of the constraint plates (10, 20, and 40 mm) were similar to those in the experiments in an effort to reproduce and verify the test results. False values of the thickness of the constraint plate (100 and 200 mm) were adopted to extend the experimental interpretation. These sham values of thickness were adopted to obtain the limiting value of restrained stress under the maximum possible amount of restraint which can be provided in the TSD. This would help in the development of an appropriate restraint-dependent stress function. The power law was implemented to investigate the effect of the constant and transient elastic modulus on the generation of restrained stress with and without creep deformation. This is given as follows:

$$J(t,\tau) = \frac{1}{E(\tau)}\left(1 + \varphi \cdot \tau^{-d}(t-\tau)^{p}\right). \quad (5)$$

To perform a transient elastic analysis, the creep coefficient '$\varphi$' was kept equal to zero to exclude the effect of creep/relaxation on the restrained stress history. The effect of the transient elastic modulus was solely realized by applying a user-supplied subroutine on the early-age elastic modulus (Fig. 10(a)). The evolution of the elastic modulus and the tensile strength of the concrete are shown in Fig. 10(a) and (b), respectively. The evolution of Young's modulus at different locations of the structure is a function of the temperature, which in turn is a function of time (Fig. 10(a)). The effect of creep/relaxation was incorporated both in the static and in the transient inelastic analyses. An analysis performed while changing the elastic modulus and creep (i.e., inelastic analysis) was best-fitted to the experimental results (Fig. 14).

### 5.4. Comparison with experimental results

A comparison of the results of the flow and the subsequent stress analysis, with respective experimental measurements, is shown in Figs. 12 and 13. Good agreement was noted between the numerical simulation and the test results, although the application of the power law model for the prediction of creep and relaxation behavior required realistic values for the parameters $\varphi$, $d$, and $p$. The use of literature values presents challenges, as specific values depend on hardening conditions such as the humidity, temperature, and the amount and type of cement. However, best-fitted values were found from a preliminary analysis. The range of the parameter values used in this study was compared to that of other investigators [28–30], and the development time '$t_d$' was taken as equal to half of the total analysis time (i.e., 15 days). Shrinkage caused by drying was prevented in the experiments; its effect was incorporated in the model values of $\varphi$, $d$, and $p$ in an implicit fashion.

A comparison was made between the various analysis types and corresponding experimental measurements (Fig. 14(a), (b)). Very low compressive stress occurred at the maximum temperature as the Young's modulus increased. If the same temperature rise was applied to hardened concrete (i.e., constant Young's modulus), the compressive stress rose. More than half of the temperature deformations did not result in compressive stress due to the slowly increasing Young's modulus in young hardening concrete. The influence of creep/relaxation occurring in hardening concrete is considerable under restraining conditions that can be 30% to 70% of autogenous shrinkage at early ages. This leads to a total reduction in the restraining stresses of nearly 50% due to stress relaxation [15,31,32]. Reduction of the

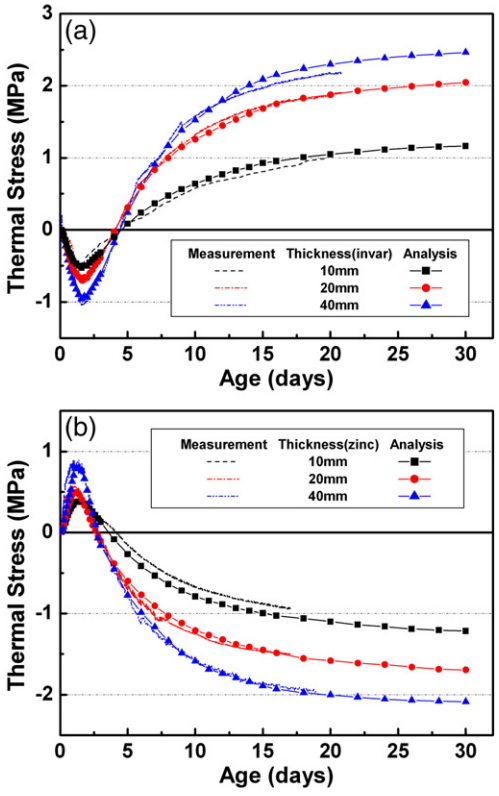


**Fig. 13.** Comparison of the stress between the experimental measurement and the numerical simulation according to varying thicknesses of the constraint materials (a) invar and (b) zinc.

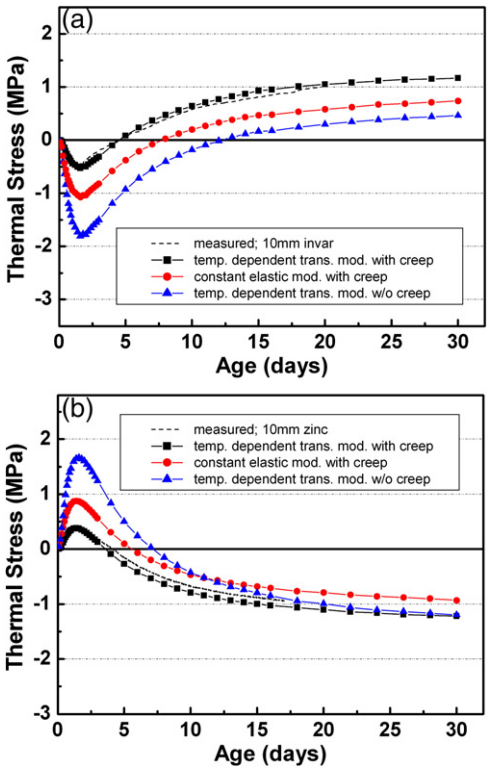


**Fig. 14.** Comparison of the stress between the measurement and various analysis conditions for the frame material with a thickness of 10 mm in (a) an invar frame (b) a zinc frame.

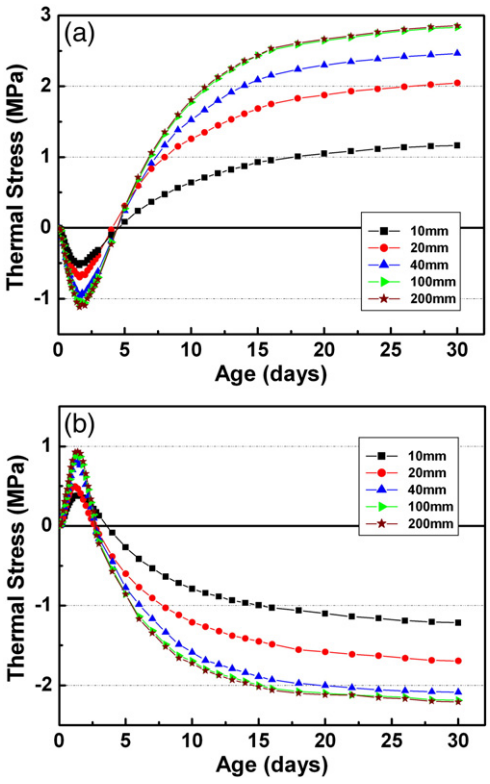


**Fig. 15.** Generation of stress from the extended numerical simulation while increasing the thickness of the restraint materials of (a) invar (b) zinc.

restrained stresses due to creep/relaxation is important in avoiding overestimation or underestimation of the actual tensile stress produced by the continuous temperature decline at later ages. Good agreement was noted between the measured and calculated stress values based on the changing elastic modulus considering the creep. A very minor difference between the measured and calculated stress values was not suitably explained, though this is believed to be due to unavoidable measurement errors, inaccuracy related to creep, or to the thermal characteristics of the concrete in this analysis.

Extended numerical results were drawn separately for each restraint material (Fig. 15(a) and (b)). The difference in the stress levels between tests involving constraint plates with thicknesses of 10 and 20 mm was pronounced but showed a gradual reduction from 20 to 200 mm (Fig. 15). Thus, the higher the restraint, the higher the residual stress. This is applicable up to a certain value of constraint plate thickness. For example, a difference of stress between 100 and 200 mm is negligible, which implies that a plate thickness equal to 200 mm offers the maximum restraint. A further increase in thickness beyond 200 mm will not increase the stress values. The thickness of the constraint plate which offered the maximum restraint (200 mm in this study) is not a practical value of constraint plate thickness. However, this value of thickness (which can provide the maximum restraint) is apt to change depending on the characteristics of different restraint materials.

The relationship between the ratio of the frame thickness and the restrained stress according to age is shown in Fig. 16(a) and (b). The ratio of the frame thickness was achieved based on the concept of normalization by assuming a thickness of the restraint plate equal to 200 mm as a reference value. A general concept of a finite element analysis was followed when determining the relationship between the ratio of the frame thickness and the restrained stresses. The degree of restraint is commonly considered to be equal to 1 (i.e., maximum) at the base of the structure and equal to zero (i.e., minimum) at the

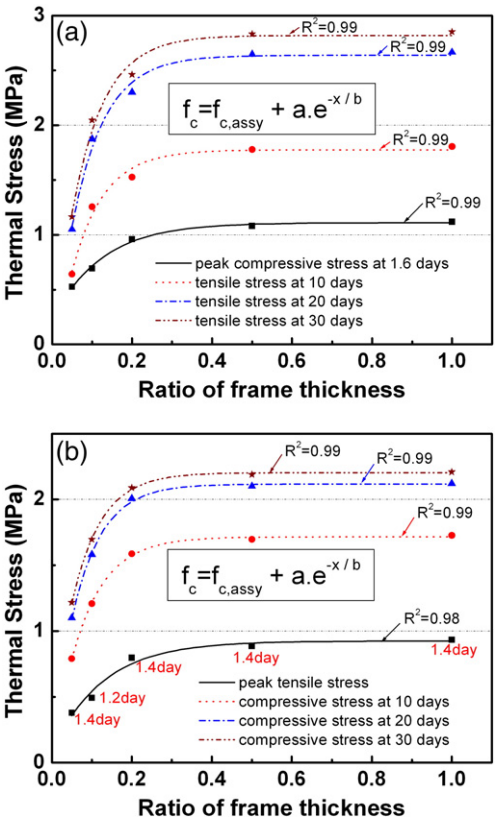


**Fig. 16.** Relationship between the stress and thickness ratio according to age of restrained concrete: (a) invar frame (b) zinc frame.

surface or top of the structure. The optimally approximated relationship between the ratio of the frame thickness and the restrained stress is given as follows:

$$f_c(x) = f_{c,assy} + a \cdot e^{-x/b}. \quad (6)$$

Here, $f_{c,assy}$ is the final asymptotic value of the restrained stress according to age; $x$ is the value of the ratio of the frame thickness, which varies along the horizontal axis; and '$a$' and '$b$' are constants that are determined from experimental data according to age.

The values of the parameters in Eq. (6) were age-dependent (Fig. 16). For all data, the obtained regression constants, $R^2$, which indicates the accuracy of the fit, were all equal to or above 98% (Fig. 16). This shows the fitness of the experimental data with the analyzed equation shown above (Eq. (6)). The values of the parameters in Eq. (6) were determined according to age. At concrete aging periods of 1.6, 10, 20, and 30 days, the corresponding asymptotic maximum restrained stress $f_{c,assy}$ was 1.11, 1.78, 2.64, and 2.82. The values of constant parameters of '$a$' were −0.89, −2.08, −2.89, and −3.03; and those for '$b$' were 0.121, 0.080, 0.081, and 0.080 for the constraint material invar (Fig. 16(a)). Similarly, for the constraint material zinc, $f_{c,assy}$ was 0.925, 1.717, 2.118, and 2.204; '$a$' was −0.84, −1.76, −2.01, and −1.96; and '$b$' was 0.126, 0.080, 0.074, and 0.073 (Fig. 16(b)).

The peak values of stress under the highest restraint were too low, even after 30 days of casting. These values were 2.85 and 2.21 MPa for the constraint materials invar and zinc, respectively. This may have been caused by the very weak restraint offered by the restraint materials used in this study or by the occurrence of micro-cracking or high early-age creep due to the thicker restraint plates. The current methodology of a thermal stress simulation can be used in applications based on the observations made during this study. It may be possible to achieve actual restraint conditions and corresponding restrained stresses according to time using the concept of reproducing the restraint conditions in the TSD.

## 6. Conclusions and recommendations

A new methodology to simulate thermal stress variation in mass concrete structures subjected to variable internal and external restraints is presented in this paper. The following conclusions are drawn from this study:

1. An accurate simulation of thermal stress under different degrees of restraint was obtained using a TSD. The risk of early-age thermal cracking should not be solely based on a temperature criterion unless effects of other parameters such as the restraining amounts and the growing early-age properties of concrete are properly incorporated when predicting the cracking stress value.
2. The influence of parameters that affect the generation of thermal stress and the resultant thermal cracking was well incorporated as the temperature and degree of stress development in restrained members can be studied simultaneously in the laboratory from the very beginning using the TSD.
3. The occurrence of plastic and drying shrinkage was minimized by maintaining a specific humidity level of 85% or more inside the chamber and by the proper wrapping of a specimen with polyester sealing film. This also helps in avoiding a condition in which the autogenous shrinkage effect is neglected during the exact measurement of the thermal stresses in special cases of typical massive concrete proportions with a $w/c$ value equal to 0.3 or less.
4. Numerical simulation of the restraint-dependent thermal stress showed good agreement with the measured results. A simplified correlation was developed between the constraint ratio and the stress development in the TSD.

A reasonable amount of agreement was achieved between the measured results and the numerical simulation. However, a detailed parametric study of the transitional effects of thermal creep should be performed, as the assumed parameters of a double power law were based on previous studies. Literature on the effects of variable thermal gradients on creep behavior is relatively scarce as it pertains to an early concrete age of five days or less. This data is needed to determine the influence of early-age creep/relaxation during a thermal stress analysis. An incorporation of improved models of the stiffness evolution and creep behavior is required as well to ascertain the authenticity of the current methodology with greater certainty. Further experiments using constraint materials with high stiffness values and lower thermal expansion coefficients are also necessary.

## Acknowledgements

This study was part of a research project supported by the Infra Structure Assessment Research Center of the Korean Ministry of Construction and Transportation (MOST) and the Research Group for Control of Crack in Concrete of the Korea Science and Engineering Foundation (KOSEF). The authors wish to express their gratitude for the financial support that has made this study possible.

## References

[1] R. de Borst, A.H. van den Boogaard, L.J. Sluys, P.A.J. van den Bogert, Computational issues in time-dependent deformation and fracture of concrete, in: Z.P. Bazant, I. Carol (Eds.), Creep and Shrinkage of Concrete, E & FN Spon, London, 1993, pp. 309–326.
[2] R. de Borst, A.H. van den Boogaard, Finite-element modeling of deformation and cracking in early-age concrete, ASCE J. Eng. Mech. 120 (12) (1994) 2519–2534.
[3] R. de Borst, P. van den Berg, Further viewpoints, analysis of creep and cracking in concrete members, in: Z.P. Bazant (Ed.), Preprints RILEM International Symposium on Creep and Shrinkage of Concrete, Mathematical Modeling, Northwestern University, Evanston, 1986, pp. 527–538.
[4] M. Eberhardt, S.J. Lokhorst, K.V. Breugel, On the reliability of temperature differentials as a criterion for the risk of early-age thermal cracking, in: R. Springenschmid (Ed.), Thermal Cracking in Concrete at Early Age, E & FN Spon, London, RILEM 1994, pp. 353–360.
[5] M. Larson, Evaluation of Restraint from Adjoining Structures, IPACS-Rep, Lulea University of Technology, Lulea, Sweden, 1999.
[6] M. Larson, Estimation of crack risk in early age concrete, Licentiate Thesis, Lulea University of Technology, Lulea, Sweden, 2000.
[7] F. Rostasy, A.-W. Gutsch, M. Kraub, Engineering Models for the Assessment of Restraint of Slabs by Soil and in Piles in the Early Age of Concrete, IPACS-Rep, Lulea University of Technology, Lulea, Sweden, 2001.
[8] J.-K. Kim, S.-E. Jeon, J.-H.J. Kim, Development of new device for measuring thermal stresses, Cem. Concr. Res. 32 (10) (2002) 1645–1651.
[9] M. Nilsson, Restraint factors and partial coefficients for crack risk analysis of early age concrete structures, Licentiate Thesis, Lulea University of Technology, Lulea, Sweden, 2003.
[10] H. Aokage, Y. Ito, N. Watanabe, Experimental study on effective modulus of elasticity in massive concrete, Trans. Jpn. Concr. Inst. 8 (1986) 119–124.
[11] R. Breitenbucher, Investigation of thermal cracking with the cracking-frame, Mater. Struct. 23 (May 3 1990) 172–177.
[12] E. Tazawa, K. Iida, Mechanism of thermal stress generation due to hydration heat of concrete, Trans. Jpn. Concr. Inst. 5 (1983) 119–126.
[13] R. Springenschmid, R. Breitenbucher, M. Mangold, Development of the cracking frame and the temperature–stress testing machine, in: R. Springenschmid (Ed.), Thermal Cracking in Concrete at Early Age, E & FN Spon, London, RILEM 1994, pp. 137–144.
[14] G. Thielen, W. Hintzen, Investigation of concrete behavior under restraint with a temperature–stress test machine, in: R. Springenschmid (Ed.), Thermal Cracking in Concrete at Early Age, E & FN Spon, London, RILEM 1994, pp. 145–152.
[15] K. Schoppel, M. Plannerer, R. Springenschmid, Determination of restraint stresses and of material properties during hydration of concrete with the temperature–stress testing machine, in: R. Springenschmid (Ed.), Thermal Cracking in Concrete at Early Age, E & FN Spon, London, RILEM 1994, pp.153–160.
[16] S.G. Park, T. Noguchi, M.H. Kim, A study on the creep and autogenous shrinkage of high performance concrete with expansive additives and shrinkage reducing admixtures at early age, Int. J. Concr. Struct. Mater. 18 (2E) (2006) 73–77.
[17] ACI Committee 207, effect of restraint, volume change, and reinforcement on cracking of mass concrete (ACI 207.2R-95), ACI Manual of Concrete Practice, American Concrete Institute, Detroit, 1995.
[18] P.E. Roelfstra, T.A.M. Salet, J.E. Kuiks, Defining and application of stress analysis-based temperature difference limits to prevent early-age cracking in concrete structures, in: R. Springenschmid (Ed.), Thermal Cracking in Concrete at Early Age, E & FN Spon, London, RILEM 1994, pp. 273–280.
[19] M. Emborg, S. Bernander, Assessment of risk of thermal cracking in hardening concrete, J. Struct. Eng. 120 (10) (1994) 2893–2912.
[20] M. Larson, Thermal crack estimation in early age concrete—Models and methods for practical application, Doctoral thesis, Lulea University of Technology, Lulea, Sweden, 2003.

[21] JCI Committee Report, A proposal of a method of calculating crack width due to thermal stress, Committee on Thermal Stress of Massive Concrete Structures, Japan Concrete Institute, Tokyo, Japan, 1992.
[22] T. Kanstad, D. Bosnjak, A.J. Overli, 3D Restraint analysis of typical structures with early age cracking problems, IPACS-Rep, Lulea University of Technology, Lulea, Sweden, 2001.
[23] M. Emborg, S. Bernander, Thermal stresses computed by a method for manual calculations, in: R. Springenschmid (Ed.), Thermal Cracking in Concrete at Early Age, E & FN Spon, London, RILEM 1994, pp. 321–328.
[24] Y. Wu, R. Luna, Numerical implementation of temperature and creep in mass concrete, Finite Elem. Analy. Des. 37 (2) (February 2001) 97–106.
[25] M. Ishikawa, Thermal stress analysis of a concrete dam, Comput. Struct. 40 (2) (1991) 347–352.
[26] DIANA User's Manual, Material Library, TNO Building and Construction Research, Delft, The Netherlands, 2003, pp. 109–113, Release 8.1.
[27] DIANA User's Manual, Analysis Procedure, TNO Building and Construction Research, Delft, The Netherlands, 2003, pp. 341–344, Release 8.1.
[28] Z.P. Bazant, E. Osman, Double power law for basic creep of concrete, Mat. Struct. 9 (January 1 1976) 3–11.
[29] K.V. Breugel, Simulation of hydration and formation of structure in hardening cement-based materials, PhD dissertation, Delft University of Technology, Delft, The Netherlands, 1991.
[30] A.M. Freudenthal, F. Roll, Creep and creep recovery of concrete under high compressive strength, ACI J. 54 (6) (1958) 1111–1142.
[31] S.A. Altoubat, D.A. Lange, Creep, shrinkage, and cracking of restrained concrete at early age, ACI Mater. J. 98 (4) (July–August 2001) 323–331.
[32] G.D. Schutter, K. Kovler, Visco-elastic response, in: A. Bentur, K. Kovler (Eds.), Early Age Cracking in Cementitious Systems, RILEM Publications S.A.R.L, Cachan Cedex, 2002, pp. 111–120.